Deuteron and Antideuteron Production in Au+Au Collisions at $\sqrt{s_{NN}}=200$ GeV

S. S. Adler,[5] S. Afanasiev,[17] C. Aidala,[5] N. N. Ajitanand,[43] Y. Akiba,[20,38] J. Alexander,[43] R. Amirikas,[12] L. Aphecetche,[45] S. H. Aronson,[5] R. Averbeck,[44] T. C. Awes,[35] R. Azmoun,[44] V. Babintsev,[15] A. Baldisseri,[10] K. N. Barish,[6] P. D. Barnes,[27] B. Bassalleck,[33] S. Bathe,[30] S. Batsouli,[9] V. Baublis,[37] A. Bazilevsky,[39,15] S. Belikov,[16,15] Y. Berdnikov,[40] S. Bhagavatula,[16] J. G. Boissevain,[27] H. Borel,[10] S. Borenstein,[25] M. L. Brooks,[27] D. S. Brown,[34] N. Bruner,[33] D. Bucher,[30] H. Buesching,[30] V. Bumazhnov,[15] G. Bunce,[5,39] J. M. Burward-Hoy,[26,44] S. Butsyk,[44] X. Camard,[45] J.-S. Chai,[18] P. Chand,[4] W. C. Chang,[2] S. Chernichenko,[15] C. Y. Chi,[9] J. Chiba,[20] M. Chiu,[9] I. J. Choi,[52] J. Choi,[19] R. K. Choudhury,[4] T. Chujo,[5] V. Cianciolo,[35] Y. Cobigo,[10] B. A. Cole,[9] P. Constantin,[16] D. d'Enterria,[45] G. David,[5] H. Delagrange,[45] A. Denisov,[15] A. Deshpande,[39] E. J. Desmond,[5] A. Devismes,[44] O. Dietzsch,[41] O. Drapier,[25] A. Drees,[44] R. du Rietz,[29] A. Durum,[15] D. Dutta,[4] Y. V. Efremenko,[35] K. El Chenawi,[49] A. Enokizono,[14] H. En'yo,[38,39] S. Esumi,[48] L. Ewell,[5] D. E. Fields,[33,39] F. Fleuret,[25] S. L. Fokin,[23] B. D. Fox,[39] Z. Fraenkel,[51] J. E. Frantz,[9] A. Franz,[5] A. D. Frawley,[12] S.-Y. Fung,[6] S. Garpman,[29,*] T. K. Ghosh,[49] A. Glenn,[46] G. Gogiberidze,[46] M. Gonin,[25] J. Gosset,[10] Y. Goto,[39] R. Granier de Cassagnac,[25] N. Grau,[16] S. V. Greene,[49] M. Grosse Perdekamp,[39] W. Guryn,[5] H.-Å. Gustafsson,[29] T. Hachiya,[14] J. S. Haggerty,[5] H. Hamagaki,[8] A. G. Hansen,[27] E. P. Hartouni,[26] M. Harvey,[5] R. Hayano,[8] N. Hayashi,[38] X. He,[13] M. Heffner,[26] T. K. Hemmick,[44] J. M. Heuser,[44] M. Hibino,[50] J. C. Hill,[16] W. Holzmann,[43] K. Homma,[14] B. Hong,[22] A. Hoover,[34] T. Ichihara,[38,39] V. V. Ikonnikov,[23] K. Imai,[24,38] D. Isenhower,[1] M. Ishihara,[38] M. Issah,[43] A. Isupov,[17] B. V. Jacak,[44] W. Y. Jang,[22] Y. Jeong,[19] J. Jia,[44] O. Jinnouchi,[38] B. M. Johnson,[5] S. C. Johnson,[26] K. S. Joo,[31] D. Jouan,[36] S. Kametani,[8,50] N. Kamihara,[47,38] J. H. Kang,[52] S. S. Kapoor,[4] K. Katou,[50] S. Kelly,[9] B. Khachaturov,[51] A. Khanzadeev,[37] J. Kikuchi,[50] D. H. Kim,[31] D. J. Kim,[52] D. W. Kim,[19] E. Kim,[42] G.-B. Kim,[25] H. J. Kim,[52] E. Kistenev,[5] A. Kiyomichi,[48] K. Kiyoyama,[32] C. Klein-Boesing,[30] H. Kobayashi,[38,39] L. Kochenda,[37] V. Kochetkov,[15] D. Koehler,[33] T. Kohama,[14] M. Kopytine,[44] D. Kotchetkov,[6] A. Kozlov,[51] P. J. Kroon,[5] C. H. Kuberg,[1,27] K. Kurita,[39] Y. Kuroki,[48] M. J. Kweon,[22] Y. Kwon,[52] G. S. Kyle,[34] R. Lacey,[43] V. Ladygin,[17] J. G. Lajoie,[16] A. Lebedev,[16,23] S. Leckey,[44] D. M. Lee,[27] S. Lee,[19] M. J. Leitch,[27] X. H. Li,[6] H. Lim,[42] A. Litvinenko,[17] M. X. Liu,[27] Y. Liu,[36] C. F. Maguire,[49] Y. I. Makdisi,[5] A. Malakhov,[17] V. I. Manko,[23] Y. Mao,[7,38] G. Martinez,[45] M. D. Marx,[44] H. Masui,[48] F. Matathias,[44] T. Matsumoto,[8,50] P. L. McGaughey,[27] E. Melnikov,[15] F. Messer,[44] Y. Miake,[48] J. Milan,[43] T. E. Miller,[49] A. Milov,[44,51] S. Mioduszewski,[5] R. E. Mischke,[27] G. C. Mishra,[13] J. T. Mitchell,[5] A. K. Mohanty,[4] D. P. Morrison,[5] J. M. Moss,[27] F. Mühlbacher,[44] D. Mukhopadhyay,[51] M. Muniruzzaman,[6] J. Murata,[38,39] S. Nagamiya,[20] J. L. Nagle,[9] T. Nakamura,[14] B. K. Nandi,[6] M. Nara,[48] J. Newby,[46] P. Nilsson,[29] A. S. Nyanin,[23] J. Nystrand,[29] E. O'Brien,[5] C. A. Ogilvie,[16] H. Ohnishi,[5,38] I. D. Ojha,[49,3] K. Okada,[38] M. Ono,[48] V. Onuchin,[15] A. Oskarsson,[29] I. Otterlund,[29] K. Oyama,[8] K. Ozawa,[8] D. Pal,[51] A. P. T. Palounek,[27] V. Pantuev,[44] V. Papavassiliou,[34] J. Park,[42] A. Parmar,[33] S. F. Pate,[34] T. Peitzmann,[30] J.-C. Peng,[27] V. Peresedov,[17] C. Pinkenburg,[5] R. P. Pisani,[5] F. Plasil,[35] M. L. Purschke,[5] A. K. Purwar,[44] J. Rak,[16] I. Ravinovich,[51] K. F. Read,[35,46] M. Reuter,[44] K. Reygers,[30] V. Riabov,[37,40] Y. Riabov,[37] G. Roche,[28] A. Romana,[25] M. Rosati,[16] P. Rosnet,[28] S. S. Ryu,[52] M. E. Sadler,[1] N. Saito,[38,39] T. Sakaguchi,[8,50] M. Sakai,[32] S. Sakai,[48] V. Samsonov,[37] L. Sanfratello,[33] R. Santo,[30] H. D. Sato,[24,38] S. Sato,[5,48] S. Sawada,[20] Y. Schutz,[45] V. Semenov,[15] R. Seto,[6] M. R. Shaw,[1,27] T. K. Shea,[5] T.-A. Shibata,[47,38] K. Shigaki,[14,20] T. Shiina,[27] C. L. Silva,[41] D. Silvermyr,[27,29] K. S. Sim,[22] C. P. Singh,[3] V. Singh,[3] M. Sivertz,[5] A. Soldatov,[15] R. A. Soltz,[26] W. E. Sondheim,[27] S. P. Sorensen,[46] I. V. Sourikova,[5] F. Staley,[10] P. W. Stankus,[35] E. Stenlund,[29] M. Stepanov,[34] A. Ster,[21] S. P. Stoll,[5] T. Sugitate,[14] J. P. Sullivan,[27] E. M. Takagui,[41] A. Taketani,[38,39] M. Tamai,[50] K. H. Tanaka,[20] Y. Tanaka,[32] K. Tanida,[38] M. J. Tannenbaum,[5] P. Tarján,[11] J. D. Tepe,[1,27] T. L. Thomas,[33] J. Tojo,[24,38] H. Torii,[24,38] R. S. Towell,[1] I. Tserruya,[51] H. Tsuruoka,[48] S. K. Tuli,[3] H. Tydesjö,[29] N. Tyurin,[15] H. W. van Hecke,[27] J. Velkovska,[5,44] M. Velkovsky,[44] V. Veszprémi,[11] L. Villatte,[46] A. A. Vinogradov,[23] M. A. Volkov,[23] E. Vznuzdaev,[37] X. R. Wang,[13] Y. Watanabe,[38,39] S. N. White,[5] F. K. Wohn,[16] C. L. Woody,[5] W. Xie,[6] Y. Yang,[7] A. Yanovich,[15] S. Yokkaichi,[38,39] G. R. Young,[35] I. E. Yushmanov,[23] W. A. Zajc,[9,†] C. Zhang,[9] S. Zhou,[7] S. J. Zhou,[51] and L. Zolin[17]

(PHENIX Collaboration)

[1]*Abilene Christian University, Abilene, Texas 79699, USA*
[2]*Institute of Physics, Academia Sinica, Taipei 11529, Taiwan*
[3]*Department of Physics, Banaras Hindu University, Varanasi 221005, India*
[4]*Bhabha Atomic Research Centre, Bombay 400085, India*

[5]*Brookhaven National Laboratory, Upton, New York 11973-5000, USA*
[6]*University of California at Riverside, Riverside, California 92521, USA*
[7]*China Institute of Atomic Energy (CIAE), Beijing, People's Republic of China*
[8]*Center for Nuclear Study, Graduate School of Science, University of Tokyo, 7-3-1 Hongo, Bunkyo, Tokyo 113-0033, Japan*
[9]*Columbia University, New York, New York 10027, USA, and Nevis Laboratories, Irvington, New York 10533, USA*
[10]*Dapnia, CEA Saclay, F-91191, Gif-sur-Yvette, France*
[11]*Debrecen University, H-4010 Debrecen, Egyetem tér 1, Hungary*
[12]*Florida State University, Tallahassee, Florida 32306, USA*
[13]*Georgia State University, Atlanta, Georgia 30303, USA*
[14]*Hiroshima University, Kagamiyama, Higashi-Hiroshima 739-8526, Japan*
[15]*Institute for High Energy Physics (IHEP), Protvino, Russia*
[16]*Iowa State University, Ames, Iowa 50011, USA*
[17]*Joint Institute for Nuclear Research, 141980 Dubna, Moscow Region, Russia*
[18]*KAERI, Cyclotron Application Laboratory, Seoul, Korea*
[19]*Kangnung National University, Kangnung 210-702, Korea*
[20]*KEK, High Energy Accelerator Research Organization, Tsukuba-shi, Ibaraki-ken 305-0801, Japan*
[21]*KFKI Research Institute for Particle and Nuclear Physics (RMKI), H-1525 Budapest 114, P.O. Box 49, Hungary*
[22]*Korea University, Seoul 136-701, Korea*
[23]*Russian Research Center, "Kurchatov Institute," Moscow, Russia*
[24]*Kyoto University, Kyoto 606-8502, Japan*
[25]*Laboratoire Leprince-Ringuet, Ecole Polytechnique, CNRS-IN2P3, Route de Saclay, F-91128, Palaiseau, France*
[26]*Lawrence Livermore National Laboratory, Livermore, California 94550, USA*
[27]*Los Alamos National Laboratory, Los Alamos, New Mexico 87545, USA*
[28]*LPC, Université Blaise Pascal, CNRS-IN2P3, Clermont-Fd, 63177 Aubiere CEDEX, France*
[29]*Department of Physics, Lund University, Box 118, SE-221 00 Lund, Sweden*
[30]*Institut für Kernphysik, University of Muenster, D-48149 Muenster, Germany*
[31]*Myongji University, Yongin, Kyonggido 449-728, Korea*
[32]*Nagasaki Institute of Applied Science, Nagasaki-shi, Nagasaki 851-0193, Japan*
[33]*University of New Mexico, Albuquerque, New Mexico 87131, USA*
[34]*New Mexico State University, Las Cruces, New Mexico 88003, USA*
[35]*Oak Ridge National Laboratory, Oak Ridge, Tennessee 37831, USA*
[36]*IPN-Orsay, Universite Paris Sud, CNRS-IN2P3, BP 1, F-91406, Orsay, France*
[37]*PNPI, Petersburg Nuclear Physics Institute, Gatchina, Russia*
[38]*RIKEN (The Institute of Physical and Chemical Research), Wako, Saitama 351-0198, Japan*
[39]*RIKEN BNL Research Center, Brookhaven National Laboratory, Upton, New York 11973-5000, USA*
[40]*St. Petersburg State Technical University, St. Petersburg, Russia*
[41]*Universidade de São Paulo, Instituto de Física, Caixa Postal 66318, São Paulo CEP05315-970, Brazil*
[42]*System Electronics Laboratory, Seoul National University, Seoul, Korea*
[43]*Chemistry Department, Stony Brook University, SUNY, Stony Brook, New York 11794-3400, USA*
[44]*Department of Physics and Astronomy, Stony Brook University, SUNY, Stony Brook, New York 11794, USA*
[45]*SUBATECH (Ecole des Mines de Nantes, CNRS-IN2P3, Université de Nantes), BP 20722-44307, Nantes, France*
[46]*University of Tennessee, Knoxville, Tennessee 37996, USA*
[47]*Department of Physics, Tokyo Institute of Technology, Tokyo 152-8551, Japan*
[48]*Institute of Physics, University of Tsukuba, Tsukuba, Ibaraki 305, Japan*
[49]*Vanderbilt University, Nashville, Tennessee 37235, USA*
[50]*Waseda University, Advanced Research Institute for Science and Engineering, 17 Kikui-cho, Shinjuku-ku, Tokyo 162-0044, Japan*
[51]*Weizmann Institute, Rehovot 76100, Israel*
[52]*Yonsei University, IPAP, Seoul 120-749, Korea*
(Received 1 June 2004; published 1 April 2005)

The production of deuterons and antideuterons in the transverse momentum range $1.1 < p_T < 4.3$ GeV/c at midrapidity in Au + Au collisions at $\sqrt{s_{NN}} = 200$ GeV has been studied by the PHENIX experiment at RHIC. A coalescence analysis, comparing the deuteron and antideuteron spectra with that of proton and antiproton, has been performed. The coalescence probability is equal for both deuterons and antideuterons and it increases as a function of p_T, which is consistent with an expanding collision zone. Comparing (anti)proton yields, $\overline{p}/p = 0.73 \pm 0.01$, with (anti)deuteron yields, $\overline{d}/d = 0.47 \pm 0.03$, we estimate that $\bar{n}/n = 0.64 \pm 0.04$. The nucleon phase space density is estimated from the coalescence measurement.

DOI: 10.1103/PhysRevLett.94.122302 PACS numbers: 25.75.Dw

Ultrarelativistic heavy-ion collisions are used to study the behavior of nuclear matter at extreme conditions of temperature and density, similar to those that existed in the universe a few microseconds after the Big Bang. Previous measurements indicate that high particle multiplicities [1] and large $\bar{p}/p$ ratios prevail at the Relativistic Heavy-Ion Collider (RHIC), which is expected for a nearly net baryon-free region [2]. As the hot, dense system of particles cools, it expands and the mean-free path increases until the particles cease interacting (''freeze-out''). At this point, light nuclei such as deuterons and antideuterons (d and $\bar{d}$) can be formed, with a probability proportional to the product of the phase space densities of its constituent nucleons [3,4]. Thus, the invariant yield of deuterons, compared to the protons [5,6] from which they coalesce, provides information about the size of the emitting system and its space-time evolution.

PHENIX [7] at RHIC is a versatile detector designed to study the production of leptons, photons, and hadrons over a wide momentum range. In this Letter, results on d and $\bar{d}$ production in Au + Au interactions at $\sqrt{s_{NN}} = 200$ GeV are presented. For the sake of brevity, in the rest of this Letter, our statements will generally apply to both particles and antiparticles.

The east central tracking spectrometer in the PHENIX detector [5,7,8] is used in this analysis. The information from the PHENIX beam-beam counters (BBCs) and zero-degree calorimeters (ZDCs) is used for triggering and event selection. The BBCs are Čerenkov counters surrounding the beam pipe in the pseudorapidity interval $3.0 < |\eta| < 3.9$, and provide the start timing signal. The ZDCs are hadronic calorimeters 18 m downstream of the interaction region and detect spectator neutrons in a narrow forward cone. Particle identification in the central rapidity region is achieved by measuring momentum (by drift chamber) and time of flight (by time-of-flight detector). The drift chamber (DC) and two layers of pad chambers are used for tracking and momentum reconstruction [8]. The time-of-flight (TOF) detector spans the pseudorapidity range $|\eta| < 0.35$ and $\Delta\phi = \pi/4$ azimuthally. The TOF consists of plastic scintillators, with a combined time resolution of $\approx$115 ps. The TOF thus provides identification of d and $\bar{d}$ in the transverse momentum (p_T) range $1.1 < p_T < 4.3$ GeV/c. For $p_T < 1.1$ GeV/c, the signal-to-background ratio suffers due to multiple scattering and energy loss effects.

The data set for this analysis includes 21.6×10^6 minimum bias events. The minimum bias cross section corresponds to $92.2^{+2.5}_{-3}\%$ of the total inelastic Au + Au cross section (6.9 b) [9]. Using the momentum determined by the DC, which has a resolution of $\delta p/p \approx 0.7\% \oplus 1\% p$ GeV/c, and the time of flight from the event vertex provided by the TOF, the mass of the particle is determined. The d and $\bar{d}$ yields are obtained by fitting the mass squared distributions to the sum of a Gaussian signal and an exponential background. Examples of mass squared distributions with fits for antideuterons in minimum bias collisions are shown in Fig. 1.

The raw yields are corrected for effects of detector acceptance, reconstruction efficiency, and detector occupancy. Corrections are determined by reconstructing single deuterons simulated using GEANT [10] and a detector response model of PHENIX, using the method described in [6]. The track reconstruction efficiency decreases in high multiplicity events because of high detector occupancy. This effect can be slightly larger for slower, heavier particles, due to detector dead times between successive hits. Occupancy effects on reconstruction efficiency ($\approx$83.5% for 0%–20% most central events) are evaluated by embedding simulated single particle Monte Carlo (MC) events in real events. Since the hadronic interactions of nuclei are not treated by GEANT, a correction needs to be applied to account for the hadronic absorption of d and $\bar{d}$ (including annihilation). The d- and the $\bar{d}$-nucleus cross sections are calculated from parametrizations of the nucleon and antinucleon cross sections:

$$\sigma_{d/\bar{d},A} = \left[\sqrt{\sigma_{N/\bar{N},A}} + \Delta_d\right]^2. \quad (1)$$

The limited data available on deuteron induced interactions [11] indicate that the term Δ_d is independent of the nuclear mass number A and that $\Delta_d = 3.51 \pm 0.25$ mb$^{1/2}$. The hadronic absorption varies only slightly over the applicable p_T range and is $\approx 10\%$ for d and $\approx 15\%$ for $\bar{d}$. The background contribution from deuterons knocked out due to the interaction of the produced particles with the beam pipe is estimated using simulations and is found to be negligible in the momentum range of our measurement.

Figure 2 shows the corrected d and $\bar{d}$ invariant yields as a function of transverse mass [m_T in the range $1.1 < p_T <$ 4.3 GeV/c, for minimum bias events, and two centrality bins: 0%–20% (most central) and 20%–92% (noncen-

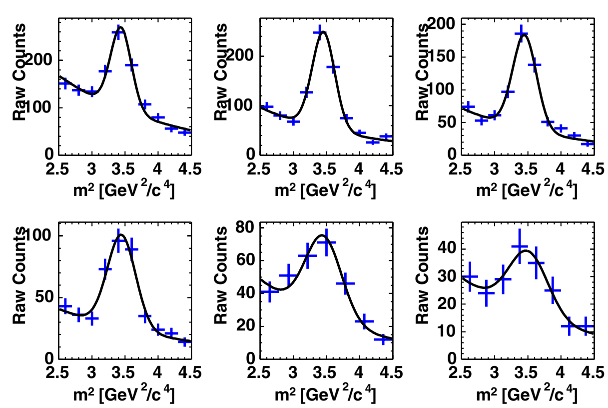

FIG. 1 (color online). Histograms of the mass squared for identified antideuterons in the transverse momentum range $1.1 < p_T < 3.5$ GeV/c (in 400 MeV/c increments), with Gaussian fits including an exponential background.

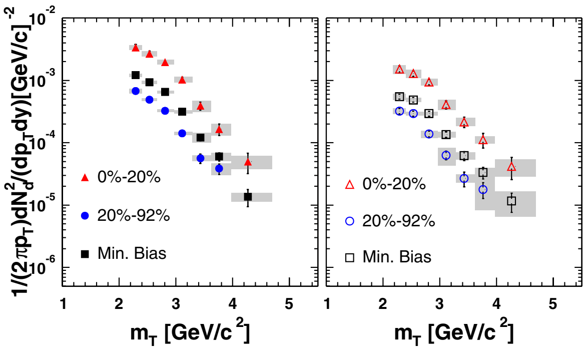

FIG. 2 (color online). Corrected spectra for deuterons (left panel) and antideuterons (right panel) for different centralities are plotted vs m_T. Error bars indicate statistical errors and gray bands the systematic errors. Values are plotted at the "true" mean value of m_T of each bin, the extent of which is indicated by the width of the gray bars along the x axis.

tral)]. The 20%–92% centrality bin is dominated by midcentral events, due to larger track multiplicities relative to peripheral events.

Systematic uncertainties have several sources: errors in particle identification, DC-TOF hit match efficiency, the uncertainty in momentum scale, d and $\bar{d}$ hadronic interaction correction, and uncertainty in occupancy corrections. All the systematic uncertainties are added in quadrature, depicted by the gray bars in Fig. 2.

The p_T spectra Ed^3N/d^3p are fitted in the range $1.1 < p_T < 3.5$ GeV/c to an exponential distribution in $m_T = \sqrt{p_T^2 + m^2}$. The inverse slopes ($T_{\rm eff}$) of the spectra are tabulated in Table I. The deuteron inverse slopes of $T_{\rm eff} =$ 500–520 MeV are considerably higher than the $T_{\rm eff} =$ 300–350 MeV observed for protons [5,6]. The invariant

TABLE I. The inverse slope parameter $T_{\rm eff}$ obtained from a m_T exponential fit to the spectra along with multiplicity dN/dy and mean transverse momentum $\langle p_T \rangle$ obtained from a Boltzmann distribution for different centralities.

$T_{\rm eff}$ [MeV]	Deuterons	Antideuterons
Minimum bias	519 ± 27	512 ± 32
0%–20%	536 ± 32	562 ± 51
20%–92%	475 ± 29	456 ± 35
dN/dy		
Minimum bias	$0.0250\pm^{0.0006(\rm stat)}_{0.005(\rm syst)}$	$0.0117\pm^{0.0003(\rm stat)}_{0.002(\rm syst)}$
0%–20%	$0.0727\pm^{0.0022(\rm stat)}_{0.0141(\rm syst)}$	$0.0336\pm^{0.0013(\rm stat)}_{0.0057(\rm syst)}$
20%–92%	$0.0133\pm^{0.0004(\rm stat)}_{0.0029(\rm syst)}$	$0.0066\pm^{0.0002(\rm stat)}_{0.0015(\rm syst)}$
$\langle p_T \rangle$ [GeV/c]		
Minimum bias	$1.54\pm^{0.04(\rm stat)}_{0.13(\rm syst)}$	$1.52\pm^{0.05(\rm stat)}_{0.12(\rm syst)}$
0%–20%	$1.58\pm^{0.05(\rm stat)}_{0.13(\rm syst)}$	$1.62\pm^{0.07(\rm stat)}_{0.1(\rm syst)}$
20%–92%	$1.45\pm^{0.05(\rm stat)}_{0.15(\rm syst)}$	$1.41\pm^{0.06(\rm stat)}_{0.15(\rm syst)}$

yields and the average transverse momenta ($\langle p_T \rangle$) are obtained by summing the data over p_T and using a Boltzmann distribution, $\frac{d^2N}{2\pi m_T dm_T dy} \propto m_T e^{-m_T/T_{\rm eff}}$, to extrapolate to low m_T regions where we have no data. The extrapolated yields constitute $\approx 42\%$ of our total yields. The rapidity distributions, dN/dy, and the mean transverse momenta, $\langle p_T \rangle$, are compiled in Table I for three different centrality bins. Systematic uncertainties in dN/dy and $\langle p_T \rangle$ are estimated by using an exponential in p_T and a "truncated" Boltzmann distribution (assumed flat for $p_T < 1.1$ GeV/c) for alternative extrapolations.

With a binding energy of 2.24 MeV, the deuteron is a very loosely bound state. Thus, the observed deuterons can be formed only at a later stage in the collision. The proton and neutron must be close in space and tightly correlated in velocity to coalesce. As a result, d and $\bar{d}$ yields are a sensitive measure of correlations in phase space at freeze-out and can provide information about the space-time evolution of the system. If deuterons are formed by coalescence of protons and neutrons, the invariant deuteron yield can be related [12] to the primordial nucleon yields by

$$E_d \frac{d^3N_d}{d^3p_d}\Big|_{p_d=2p_p} = B_2\left(E_p \frac{d^3N_p}{d^3p_p}\right)^2, \tag{2}$$

where B_2 is the coalescence parameter, with the subscript implying that two nucleons are involved in the coalescence. The above equation includes an implicit assumption that the ratio of neutrons to protons is unity. The proton and antiproton spectra [6] are corrected for feed-down from Λ and $\bar{\Lambda}$ decays by using a MC simulation tuned to reproduce the particle ratios: (Λ/p and $\bar{\Lambda}/\bar{p}$) measured by PHENIX at 130 GeV [13].

Figure 3 displays the coalescence parameter B_2 as a function of p_T for different centralities. Thermodynamic models [4] predict that B_2 scales with the inverse of the effective volume $V_{\rm eff}$ ($B_2 \propto 1/V_{\rm eff}$). The lower B_2 in more central collisions may thus reflect the increase in the participant volume with centrality. We also observe that B_2 increases with p_T. This is consistent with an expanding

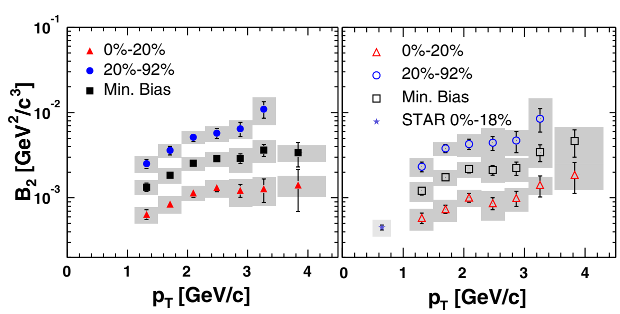

FIG. 3 (color online). Coalescence parameter B_2 vs p_T for deuterons (left panel) and antideuterons (right panel). Gray bands indicate the systematic errors. Values are plotted at the true mean value of p_T of each bin, the extent of which is indicated by the width of the gray bars along the x axis.

source because position-momentum correlations lead to a higher coalescence probability at larger p_T. The p_T dependence of B_2 can provide information about the density profile of the source as well as the expansion velocity distribution. It has been shown [14,15] that a Gaussian source density combined with a linear flow velocity profile leads to a constant B_2 with p_T. This is not supported by our data, which show a rise in B_2 with p_T. An increase of B_2 with p_T can be achieved if the Gaussian source density is replaced with a flat distribution [14,15]. The increase is a consequence of the flat density distribution giving greater weight to the outer parts of the system where the flow is strongest when a linear velocity profile is used.

Figure 4 compares B_2 for most central collisions to results at lower $\sqrt{s}$ [16–21]. Note that B_2 is nearly independent of $\sqrt{s}$, indicating that the source volume does not change appreciably with center-of-mass energy (with the caveat that B_2 varies as a function of p_T, centrality, and rapidity). This observation is consistent with what has been observed in Bose-Einstein correlation Hanbury Brown-Twiss analysis at RHIC [22] for identified particles. The coalescence parameter B_2 for d and $\bar{d}$ is equal within errors, indicating that nucleons and antinucleons have the same temperature, flow, and freeze-out density distributions.

The $\bar{d}/d$ ratio is independent of centrality and p_T within errors. The average value of $\bar{d}/d$ is 0.47 ± 0.03, consistent with the square of the ratio $\bar{p}/p = 0.73 \pm 0.01$ [6] within statistical and systematic uncertainties. This is expected if deuterons are formed by coalescence of comoving nucleons and $\bar{p}/p = \bar{n}/n$. The ratio $\bar{n}/n$ can, however, be estimated from the data based on the thermal chemical model. Assuming thermal and chemical equilibrium, the chemical fugacities are determined from the particle/antiparticle ratios [14]:

$$\frac{E_A(d^3N_A/d^3p_A)}{E_{\bar{A}}(d^3N_{\bar{A}}/d^3p_{\bar{A}})} = \exp\left(\frac{2\mu_A}{T}\right) = \lambda_A^2. \qquad (3)$$

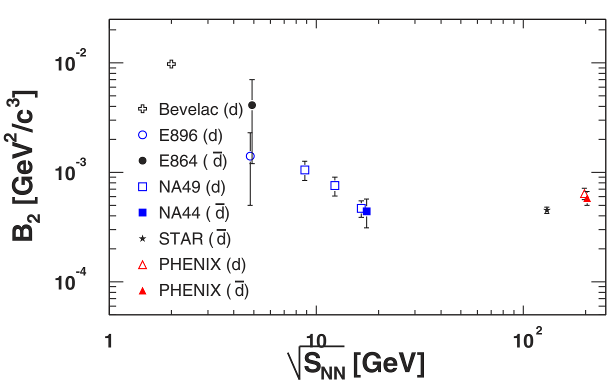

FIG. 4 (color online). Comparison of the coalescence parameter for deuterons and antideuterons ($p_T = 1.3$ GeV$/c$) with other experiments at different values of $\sqrt{s}$.

Using the ratio $p/\bar{p}$, the extracted proton fugacity is $\lambda_p = \exp(\mu_p/T) = 1.17 \pm 0.01$. Similarly, using the $d/\bar{d}$ ratio, the extracted deuteron fugacity is $\lambda_d = \exp[(\mu_p + \mu_n)/T] = 1.46 \pm 0.05$. From this, the neutron fugacity can be estimated to be $\lambda_n = \exp(\mu_n/T) = 1.25 \pm 0.04$, which results in $\bar{n}/n = 0.64 \pm 0.04$. The extracted $\bar{p}/p$ and $\bar{n}/n$ ratios are in agreement with what one would expect from the initial neutron excess in the Au nucleus if the same number of (anti)neutrons and (anti)protons are produced in the collision. Thermal models predict [23] $\bar{d}/d = 0.52$ and $\bar{n}/n = 0.73$ for $T = 177$ MeV and $\mu_B = 29$ MeV.

Finally, the coalescence requirement allows us to estimate the nucleon phase space distribution, i.e., the average number of nucleons per cell $(d^3pd^3x)/h$ in phase space. We define the phase space distribution averaged over the source volume as

$$\langle f(p)\rangle = \frac{1}{2S+1}\frac{(2\pi\hbar)^3}{V}\frac{d^3N}{dp^3}, \qquad (4)$$

where $2S + 1$ is the spin degeneracy factor. From the coalescence equation [15], $f_A(\vec{r},\vec{p}) = [f(\vec{r},\vec{p}/A)]^A$, we can thus calculate $\langle f\rangle$ as a function of p_T from the measured invariant yields, if we assume that the protons, neutrons, and deuterons are emitted from the same volume. The results are shown in Fig. 5. The phase space density is well below 1 in the range of our measurement, and much lower than what has been found for pions produced in Au + Au collisions previously [24].

To summarize, the transverse momentum spectra of d and $\bar{d}$ in the range $1.1 < p_T < 4.3$ GeV$/c$ have been measured at midrapidty in Au + Au collisions at $\sqrt{s_{NN}} =$ 200 GeV, and are found to be less steeply falling than proton (and antiproton) spectra. The extracted coalescence parameter B_2 increases with p_T, which is indicative of an expanding source. The results rule out a Gaussian source density distribution combined with a linear flow velocity profile and seem to favor a flat density distribution. The B_2 measured in nucleus-nucleus collisions is independent of $\sqrt{s_{NN}}$ above 12 GeV, consistent with the energy depen-

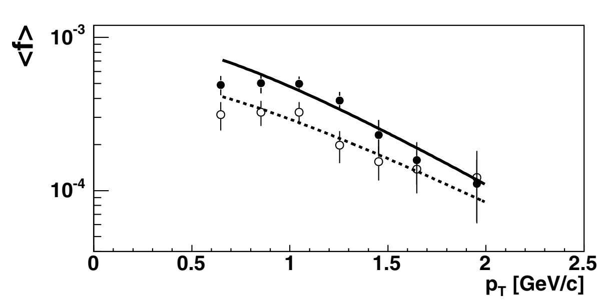

FIG. 5. Average nucleon phase space density as a function of p_T for central collisions. Solid circles correspond to nucleons and open circles correspond to antinucleons. The curves are fits to a Boltzmann function, $C\exp(-m_T/T)$, with $T = 568 \pm 96$ MeV (nucleons) and $T = 670 \pm 182$ MeV (antinucleons).

dence of the source radii extracted from Bose-Einstein correlation measurements. B_2 is equal within errors for both deuterons and antideuterons. From the measurements, it is estimated that $\bar{n}/n = 0.64 \pm 0.04$.

We thank the staff of the Collider-Accelerator and Physics Departments at BNL for their vital contributions. We acknowledge support from the Department of Energy and NSF (USA), MEXT and JSPS (Japan), CNPq and FAPESP (Brazil), NSFC (China), CNRS-IN2P3 and CEA (France), BMBF, DAAD, and AvH (Germany), OTKA (Hungary), DAE and DST (India), ISF (Israel), KRF and CHEP (Korea), RMIST, RAS, and RMAE, (Russia), VR and KAW (Sweden), U.S. CRDF for the FSU, U.S.-Hungarian NSF-OTKA-MTA, and U.S.-Israel BSF.

*Deceased.
†PHENIX Spokesperson.
Electronic address: zajc@nevis.columbia.edu

[1] K. Adcox *et al.*, Phys. Rev. Lett. **86**, 3500 (2001); B. B. Back *et al.*, Phys. Rev. Lett. **88**, 022302 (2002).
[2] K. Adcox *et al.*, Phys. Rev. Lett. **88**, 242301 (2002); B. B. Back *et al.*, Phys. Rev. C **67**, 021901 (2003); C. Adler *et al.*, Phys. Rev. Lett. **86**, 4778 (2001).
[3] L. P. Csernai and J. I. Kapusta, Phys. Rep. **131**, 223 (1986).
[4] A. Z. Mekjian, Phys. Rev. C **17**, 1051 (1978).
[5] K. Adcox *et al.*, Phys. Rev. C **69**, 024904 (2004).
[6] S. S. Adler *et al.*, Phys. Rev. C **69**, 034909 (2004).
[7] K. Adcox *et al.*, Nucl. Instrum. Methods Phys. Res., Sect. A **499**, 469 (2003), and references therein.
[8] J. T. Mitchell *et al.*, Nucl. Instrum. Methods Phys. Res., Sect. A **482**, 491 (2002).
[9] S. S. Adler *et al.*, Phys. Rev. Lett. **91**, 072301 (2003).
[10] GEANT 3.21, CERN program library.
[11] J. Jaros *et al.*, Phys. Rev. C **18**, 2273 (1978); E. O. Abdurakhmanov *et al.*, Z. Phys. C **5**, 1 (1980).
[12] S. T. Butler and C. A. Pearson, Phys. Rev. **129**, 836 (1963).
[13] K. Adcox *et al.*, Phys. Rev. Lett. **89**, 092302 (2002).
[14] R. Scheibl and U. Heinz, Phys. Rev. C **59**, 1585 (1999).
[15] A. Polleri, J. P. Bondorf, and I. N. Mishustin, Phys. Lett. B **419**, 19 (1998).
[16] S. Wang *et al.*, Phys. Rev. Lett. **74**, 2646 (1995).
[17] S. Albergo *et al.*, Phys. Rev. C **65**, 034907 (2002).
[18] T. A. Armstrong *et al.*, Phys. Rev. Lett. **85**, 2685 (2000).
[19] T. Anticic *et al.*, Phys. Rev. C **69**, 024902 (2004).
[20] I. G. Bearden *et al.*, Phys. Rev. Lett. **85**, 2681 (2000).
[21] C. Adler *et al.*, Phys. Rev. Lett. **87**, 262301 (2001).
[22] K. Adcox *et al.*, Phys. Rev. Lett. **88**, 192302 (2002); C. Adler *et al.*, Phys. Rev. Lett. **87**, 082301 (2001).
[23] P. Braun-Munzinger, D. Magestro, K. Redlich, and J. Stachel, Phys. Lett. B **518**, 41 (2001); J. Stachel (private communication).
[24] F. Laue *et al.*, Nucl. Phys. **A698**, 177c (2002).